

Supplementary Information for Shin *et al.*

Supplementary Methods

Supplementary Text

Supplementary Figure Legends

Text for Supplementary Movies (1-12)

References

Supplementary Figures

SUPPLEMENTARY METHODS

Reagents

ML-7, human fibrinogen and human serum albumin (low endotoxin) were from Sigma-Aldrich. Y-27632 and latrunculin B were from Calbiochem. fMLP was from BioChemika. Human fibronectin was from BD Biosciences. Human recombinant ICAM-1 was from R&D Systems. Alexa fluor 488 phalloidin and rhodamine-phalloidin were from Molecular Probes. ON-TARGETplus SMARTpool siRNAs containing four siRNAs specifically targeting human MLCK, non-specific siRNAs and siGLO were from Dharmacon. The GRADSP and GRGDSP peptides were from Biomol. Mouse or rabbit anti-MLCK antibodies were from Sigma-Aldrich or generated as described ¹. Rabbit anti-nonmuscle myosin II heavy chain A and B antibody were from Covance (Emeryville, CA). Mouse anti-GST antibody was from Santa Cruz Biotechnology. Rabbit anti-phospho [Ser19] myosin light chain antibody, rabbit anti-Akt antibody, and rabbit anti-phospho [Ser473]-Akt antibody were from Cell Signaling Technology. Calcein AM and DiO were from Invitrogen.

DNA Constructs

EGFP-tagged sMLCK construct was a gift from Anne Bresnick (Albert Einstein College of Medicine)². EGFP-tagged $\alpha 5$ integrin³ and mCherry-tagged myosin IIA⁴ were kindly provided by Dr. Rick Horwitz (University of Virginia). GFP-actin was from Clontech. Information on PAK-PBD-YFP and PH-AKT-YFP was reported^{5,6}. GST-FN III₉₋₁₁ was also described⁷.

Western Blotting

For western analysis of phospho-Akt, cells (with or without 25 μ M ML-7) were resuspended in modified HBSS (mHBSS) and stimulated with or without 1 μ M fMLP at RT. Stimulation was stopped by the addition of 2X Laemmli sample buffer containing a cocktail of protease inhibitors. Equal amounts of protein lysates were loaded on reducing SDS-PAGE gels. After electrophoresis, gels were immunoblotted with anti-phospho [Ser473]-Akt antibody (1:200). To determine total Akt, rabbit anti-Akt antibody was used (1:1000). To determine total levels of proteins in neutrophils, cells without fMLP or ML-7 treatment were used. Antibodies included mouse anti-MLCK (1:1000), anti-non-muscle myosin II heavy chain A (1:500), and anti-nonmuscle myosin II heavy chain B (1:500).

Rac Activation Assay

To determine Rac-GTP levels in dHL-60 lysate, we used an absorbance-based (490 nm) Rac G-LISA kit (Cytoskeleton, Inc). dHL-60 cells were preincubated for 30 min with ML-7 (25 μ M), centrifuged for 5 min at 2,000 rpm at RT, resuspended in mHBSS (2×10^6 cells in 0.5 ml per condition), and stimulated or unstimulated with 100 nM fMLP. The reaction was stopped by the addition of 0.5 ml of 2X lysis buffer (provided with the kit) at 4°C. Subsequent steps were performed as described in the protocol attached to the kit.

Lentivirus-mediated myosin IIA knockdown

The pKLO.1-puro lentiviral vectors containing scramble or myosin IIA-targeting shRNAs were purchased from Sigma. We used the Viralpower Lentivirus Packaging System (Invitrogen) to generate lentivirus according to the manufacturer's instructions. Briefly, HEK293T cells were plated and transfected on the second day with shRNA-containing plasmids using the Fugene 6 reagent (Roche). The medium was replaced the next day with the virus packaging medium containing DMEM, 30% FBS, 1 mM sodium pyruvate, 4 mM glutamine. Supernatant containing the lentivirus was collected after 48-72 h and was concentrated with ultracentrifugation (20,000 rpm, 1 h).

Concentrated viruses were added to differentiating HL-60 cells (day 2 after differentiation) and incubated for 12 h. A multiplicity of infection (MOI) of 100 was used. Polybrene (6 µg/mL) (Sigma) was also added to the medium to improve the infection efficiency. Virus-containing medium was replaced with fresh culture medium, and cells were continuously cultivated for 4-5 d before subsequent analyses.

Confocal Fluorescence Microscopy and 3D Reconstruction

Confocal optical sectioning was performed with an Andor Technology Revolution System Spinning Disk Confocal Microscopy system (Andor) coupled to an Olympus IX71 inverted microscope with Olympus 100x APO/1.4 NA objective. The refraction index of immersion media was 1.515. Theoretical *xy*- and *z*-axes resolutions were 0.159 and 0.2 µm, respectively. Images were obtained using iXon EM+ DU-897 back illuminated EMCCD (Andor Technology). Confocal images were taken with 0.2 µm step size. Upon acquisition, the confocal images were deconvoluted with Autoquant

X 2.1 software (Media Cybernetics, Inc., Silver Spring MD). The 3D structure of the actomyosin network was reconstructed from the deconvoluted images using IMARIS software (Bitplane).

Measurement of Polymerized Actin

The procedure for measuring polymerized actin has already been described ^{8,9}. Briefly, cells (pretreated with or without ML-7, 30 min) were stimulated in mHBSS in suspension with 1 μ M fMLP at RT. After fixation by 2% paraformaldehyde for 20 min at 4°C, cells were permeabilized with 0.2% Triton X-100 and stained with 0.2 μ M rhodamine-phalloidin for 30 min on ice. Stained cells were resuspended in ice-cold PBS, and fluorescence was determined by flow cytometry with a BD Biosciences LSR II System. The mean fluorescence intensity of the cell population was determined.

Adhesion Assay

Neutrophil adhesion to 96-well tissue culture plate was evaluated as described by Ryu *et al.* ¹⁰. After stimulation by chemoattractant, cells pretreated with or without ML-7 were allowed to adhere to a 96 well-plate coated with fibronectin (100 μ g/ml) and blocked with 2% BSA in PBS, at 37°C for 30 min. Non-adherent cells were removed by washing, and adherent cells were fixed with 3.7% PFA and stained with crystal violet (0.1% in 10% methanol). Stained cells were thoroughly washed and lysed with 1% SDS, and the absorbance from each sample was measured at 590 nm by a microplate reader (SpectraMax M2).

Micropipette Assay in Suspension

The procedure was modified from a previous report ¹¹. Micropipettes for holding a cell and applying chemoattractant were mounted on the microscope stage. Eppendorf's programmable micromanipulator,

the TransferMan NK 2, was used in the holding (left) side, while Injectman NI 2 was used for application of chemoattractant (right side). A single, round non-stimulated neutrophil was held in a holding pipette with an internal diameter of 5 μm (World Precision Instruments). Another pipette with an internal diameter of 1 μm was filled with 10 μM fMLP and positioned 5 μm from the cell surface. Suspended cells were gently held with CellTram Air connected to TransferMan NK 2 while precise delivery of chemoattractants was carried out from the right side with CellTram Vario. Chemoattractant-containing solution was blown over the cell, which initiated the extension of a single pseudopod. Pseudopod extension was observed in an inverted microscope (Leica DM IRE2) with a 40X objective. Images were captured with a charge-coupled device camera (Hamamatsu, C4742-95-12ERG) and analyzed with ImageJ software. The rate of pseudopod extension was calculated from the measured pseudopod lengths in time lapses.

SUPPLEMENTARY TEXT

Expression of MLCK proteins in human neutrophils

We examined the expression of MLCK in primary neutrophils and dHL-60 cells. Western blotting indicated that both cells mainly expressed the ~130-kD short form of MLCK (Figure S4A); the 210-kD long form was nearly undetectable. This pattern was similar to that in human T lymphocytes¹², suggesting that predominance of the short MLCK form may be common to leukocytes.

Upon fMLP stimulation of dHL-60 cells, sMLCK-EGFP translocated from the cytosol to the plasma membrane within 30–45 sec (Figure S4B; Supplementary Movies S10 and S11). As cells polarized morphologically, typically by 2–3 min, sMLCK-EGFP was recruited to the leading edge. The asymmetric recruitment of MLCK was also seen in cells polarizing and moving toward a point source of fMLP delivered by micropipette (Figure S4C). Furthermore, MLCK asymmetry was not caused by increased amounts of membrane in ruffles at the front, because the GFP-tagged N-terminal fragment of protein Lyn (24 amino acids; Lyn24-GFP)¹³, which associates with the plasma membranes via myristoylation and palmitoylation, was distributed uniformly around the plasma membranes (Figure S4D).

MLCK depletion mimics the effects of ML-7 treatment

To rule out non-specific actions caused by ML-7, we used RNAi-mediated MLCK knockdown to deplete MLCK and study its effects. The Amaxa Nucleofection System allowed us to deliver siRNAs into nearly all the cells after transfected and was used to transiently express siRNAs that selectively target MLCK (Figure S7A and S7B). The efficacy of the siRNAs to deplete MLCK was confirmed by assessing the level of endogenous MLCK, in the presence of either non-targeting siRNAs or siRNAs

against MLCK (Figure S7A). MLCK depletion induced dHL-60 cells to exhibit defects in protrusion and migration similar to those caused by ML-7, whereas the non-targeting siRNAs exerted no effects (Figure S7C-S7D).

Notably, the migratory defects in cells treated with ML-7 or with MLCK depleted were more severe than mouse neutrophils deficient in MYLK, the 210 kD isoform of MLCK ¹⁴. When plated on fibrinogen and exposed to chemoattractants, the MYLK-deficient mouse neutrophils polarized normally, migrated faster than the wild-type cells, but frequently changed direction. A possible explanation for the discrepancy is that ML-7 or siRNAs targets both isoforms of MLCK in dHL-60 cells while only the 210 kD form is deleted in MYLK-deficient mouse neutrophils ¹⁴.

MLCK inhibition or depletion impairs the frontness signals

We previously showed that the leading-edge activity is mediated by the frontness signaling pathway ^{5,6,15}. To provide a mechanistic explanation for the defects caused by MLCK inhibition and depletion, we assessed the effect of MLCK inhibition on frontness signals by monitoring the behavior of PH-AKT-GFP (GFP-tagged PH domain of the protein kinase Akt/PKB, readout for PI3Ps ¹⁶), PAK-PBD-YFP (yellow fluorescence protein-tagged p21-binding domain of PAK, readout for Rac-GTP in dHL-60 cells ¹⁵), and actin-YFP in living cells with or without MLCK inhibition. As described earlier, an fMLP gradient delivered by a micropipette induced cells to polarize and migrate persistently towards the tip of the micropipette (Figure S8A, left panels). Upon fMLP stimulation, these fluorescent probes translocated from cytosol and accumulated at the leading edge of chemotaxing cells. The recruitment of PI3Ps, Rac-GTP and polymerized actin in pseudopods was robust and stable, as indicated by both the loss of cytosolic GFP (or YFP) signals after stimulation and their strong asymmetric localization at

the neutrophil's leading edge during migration. A quantitative analysis of the asymmetry in fluorescence intensity across the cells revealed a steep gradient of the fluorescent signal in untreated control cells (61, 85, and 67% decrease for PH-AKT-GFP, PAK-PBD-YFP and actin-YFP over a distance of 10 μ m, respectively) (Figure S8B). In contrast, ML-7-treated cells under the same conditions exhibited poor leading edge recruitment of PH-AKT-GFP, PAK-PBD-YFP and actin-YFP, as reflected by much smaller gradients (21, 36, and 11%, respectively) (Figure S8A and S8B). Moreover, when compared with control cells, ML-7-treated cells exhibited a marked reduction (30–50%) in the ratio of mean fluorescence intensity between the leading edge and cytosol (i.e., mean intensity at front/mean intensity at the back), again revealing an impaired asymmetric recruitment of the frontness markers (Figure S8C). The use of ratio of mean fluorescence intensity discounts the variations in the levels of fluorescence probes among cells and is thus more appropriate for assessing the relative accumulation of the fluorescent signals at the leading edge. Similar to ML-7 treatment, MLCK depletion also impaired the recruitment of the frontness markers (Fig. S7E).

Inhibition of adhesion prevents leading-edge establishment and stability

MLCK-inhibited fibroblasts exhibit defects in assembly¹⁷ or turnover¹⁸ of focal adhesions. Cell adhesion sites are required to stabilize leading edges and promote cell polarity¹⁹. To assess the role of adhesion in regulating neutrophil polarity during chemotaxis, we plated dHL-60 cells on fibronectin and then treated them with a soluble RGD peptide that inhibits binding of α 5 β 1-integrin to fibronectin (α 5 β 1 integrins are the main fibronectin receptors in neutrophils²⁰) before fMLP stimulation. This procedure allowed us to selectively prevent fMLP-induced de novo adhesion. An RAD peptide was used as a negative control. With a point source of fMLP in the presence of RAD peptide, dHL-60 cells migrated to the pipet tip and maintained a highly polarized morphology with well-developed

pseudopods (Figure S12A and S12B). In contrast, cells treated with the RGD peptide only transiently polarized in response to fMLP, with much smaller and less stable leading edges that often retracted after protrusion, resulting in a less polarized, slowly migrating cell (Figure S12A-12C). Thus, blocking cell adhesion caused defects that mirrored those caused by MLCK inhibition (Figure 3B).

SUPPLEMENTARY FIGURE LEGENDS

Supplementary Figure S1. (A) The average tractions at the leading (front) and the trailing edge (back) of a chemotaxing dHL-60 cell. The graph shows part (~18 sec) of the whole migratory response. x axis indicates time in sec. y axis is in Pascal (Pa). (B) PSD plots of tractions at the leading (left panel) and the trailing edge (right panel) of three migratory dHL-60 cells. Traction values from three cells were analyzed and combined in one plot. See Figure 1 legends for more details.

Supplementary Figure S2. (A) Western blot analysis of myosin II heavy chain isoform A (MHCIIA) and B (MHCIIIB) in human primary neutrophils and dHL-60 cells. Embryonic stem cells (human; denoted as hESC) expressed both myosin IIA and IIB and were used as a positive control. α -tubulin was used as a loading control. (B) Schematic view of myosin IIA localization in a polarized neutrophil after fMLP stimulation. The representation shows a cross-section of the neutrophil and is based on confocal fluorescence microscopy combined with 3D reconstruction. The movies showing 3D views of myosin IIA immunofluorescence are available (Supplementary Movies S4 and S5). (C) PSD plots of tractions at the leading (left panel) and the trailing edge (right panel) of three dHL-60 cells treated with blebbistatin (100 μ M, 30 min). Traction values from three cells were analyzed and combined in one plot. See Figure 2 legends for more details. (D) PSD plots of tractions at the leading (left panel) and the trailing edge (right panel) of a primary neutrophil treated with blebbistatin (100 μ M, 30 min). 5 cells were analyzed, and a representative cell is shown.

Supplementary Figure S3. (A and B) Speed of protrusion (A) and retraction frequency (B) of the leading edge in cells responding to a gradient of fMLP delivered by a micropipette. dHL-60 cells were not pretreated (control), pretreated with blebbistatin (Blebbis, 100 μ M, 30 min), infected with

lentivirus containing myosin IIA-targeting shRNAs (MyoII KD), or pretreated with Y-27632 (30 μ M, 30 min). The value are means \pm SEM (n = 27 for control, 26 for cells treated with Blebbistatin, 24 for myosin IIA-depleted cells, and 28 for cells treated cell Y-27632. Student t tests compared data between experimental groups. Results significantly different from those of control are indicated by asterisks (*, $p < 0.0001$; **, $p < 0.001$). **(C and D)** Percentage of dHL-60 cells demonstrating leading-edge retractions **(C)** and long stretched tails **(D)** when exposed to fMLP gradients. Cells retracting their leading edges at least once during migration were scored as positive. To define cells with long tails, we calculated ratios between the length and width in individual cells and used 2 as a cut-off value. Each bar represents the mean+SEM (error bars) of different numbers of cells that were tested in multiple experiments: 30 control cells and 27, 24, and 30 cells for blebbistatin, myosin IIA depletion, and Y-27632, respectively. Asterisks indicate that the value for cells with the treatments differs from the corresponding control by $p < 0.0001$. **(E-H)** The same set of analysis for primary human neutrophils, which were not pretreated (control), pretreated with blebbistatin (Blebbis, 100 μ M, 30 min), or pretreated with Y-27632 (30 μ M, 30 min). The value are means \pm SEM (n = 19 for control, 21 for cells treated with Blebbistatin, and 18 for cells treated cell Y-27632. Student t tests compared data between experimental groups. Results significantly different from those of control are indicated by asterisks (*, $p < 0.0001$). **(I)** Western blot of myosin IIA in dHL-60 cells with or without myosin IIA depletion. Infection of cells with viruses containing three separate myosin IIA-targeting sequences effectively depleted myosin IIA, when compared with cells without infection (no infect.) or cells infected with viruses containing a scramble shRNA or three myosin IIA-specific shRNAs. The shRNA sequence 29464 was used in Fig. 2F. α -tubulin was a loading control. A typical experiment from four separate experiments is shown.

Supplementary Figure S4. (A) Western blotting of primary human neutrophils and dHL-60 cells with mAbs specific for MLCK. α -tubulin was used as a loading control. (B) dHL-60 cells were transfected with sMLCK-EGFP and exposed for the indicated times to the uniform concentration of fMLP (1 μ M). sMLCK-EGFP fluorescence and the corresponding DIC images are shown. Arrows point to the recruitment of sMLCK-EGFP. $n = 31$ cells. (C) dHL-60 cells were transfected with sMLCK-EGFP and exposed for the indicated times to 10 μ M fMLP from a micropipette. sMLCK-EGFP fluorescence and corresponding DIC images are shown. $n > 15$ cells. Bars, 10 μ m. Arrows point to the recruitment of sMLCK-EGFP. Movie of the cells in (C) is available (Supplementary Movies S10 and S11). (D) dHL-60 cells were transfected with Lyn24-GFP and stimulated by a micropipette containing 10 μ M fMLP for the indicated times. GFP fluorescence and the corresponding DIC images are shown. The arrow points to a migrating cell with uniform distribution of Lyn24-GFP. Bar, 10 μ m.

Supplementary Figure S5. (A) Primary neutrophils were pretreated with or without ML-7 (25 μ M, 30 min) prior to the exposure to an attractant supplied by a micropipette containing 10 μ M fMLP. The four images in each row show the positions of representative cells (each identified with a superimposed letter) after the indicated times of exposure to fMLP. The white arrow points to the poorly-developed leading edge. Bars, 10 μ m. (B and C) Speed of protrusion (B) and retraction frequency (C) of the leading edge in primary neutrophils responding to a gradient of fMLP delivered by a micropipette. Cells were pretreated with or without ML-7. The values are means \pm SEM ($n = 21$ for control, 22 for cells treated with ML-7). Student t tests compared data between experimental groups. Results significantly different from those of control are indicated by asterisks (**; $p < 0.001$).

Supplementary Figure S6. (A) Before exposure to attractant supplied by a micropipette containing 10 μ M fMLP, cells plated on fibrinogen (denoted as FG) were not pretreated (control) or pretreated with ML-7 (25 μ M, 30 min). The three images in each row show the positions of individual cells (each identified with a superimposed letter) after the indicated times of exposure to fMLP. Yellow arrows point to the position of micropipettes, which are out of focus. Bar, 10 μ m. (B and C) Speed of protrusion (B) and retraction frequency (C) of the leading edge in cells on fibrinogen responding to a gradient of fMLP delivered by a micropipette. dHL-60 cells were not pretreated (control) or pretreated with ML-7. The value are means \pm SEM (n = 22 for control, 21 for cells treated with ML-7. Student t tests compared data between experimental groups. Asterisks indicate that the value for cells with ML-7 treatment differs from the corresponding control by $p < 0.0001$.

Supplementary Figure S7. (A) dHL-60 cells were transfected with pooled siRNAs which are specifically targeting human MLCK or non-targeting and blotted for MLCK (left panel). α -tubulin is a loading control. Right panel: relative level of endogenous MLCK is measured after transfecting each siRNA constructs. Values are means \pm SEM (n = 3). Results significantly different from those of control are indicated by asterisks (*, $p < 0.05$). (B) dHL-60 cells were co-transfected with siGLO Red and pooled siRNAs that are either non-targeting or specifically targeting human MLCK at the ratio of 1:5. 48 hrs after transfection, images were collected to check the transfection efficiency of siRNAs into dHL-60 cells. Only images of cells co-transfected with siGLO and non-targeting siRNAs are shown. Bar, 10 μ m. (C and D) dHL-60 cells which were transfected with pooled siRNAs that are either non-targeting or specifically targeting human MLCK were exposed to a chemotactic gradient delivered from a micropipette containing 10 μ M fMLP for 5 min. Speed of protrusion (C) and retraction frequency (D) of the leading edge in cells responding to the gradient throughout the

observed time period. The results are shown in the graph ($n = 49$ for non-targeting siRNA-transfected cells, 56 for MLCK-specific siRNA-transfected cells). Results significantly different from those of control are indicated by asterisks (*, $p < 0.001$; **, $p < 0.0001$). MLCK depletion caused similar protrusion and migration defects when cells were stimulated on fibrinogen (data not shown). **(E)** dHL-60 cells co-transfected with actin-YFP and siRNAs (either non-targeting or specifically targeting human MLCK) were exposed to a chemotactic gradient delivered from a micropipette containing 10 μ M fMLP for the times indicated. Fluorescence images of actin-YFP and the corresponding DIC images are shown. ($n = 14$ for non-targeting siRNA-transfected cells, 11 for MLCK-specific siRNA-transfected cells). Bar, 10 μ m.

Supplementary Figure S8. **(A)** dHL-60 cells transfected with actin-YFP (top), PAK-PBD-YFP (middle), or PH-AKT-GFP (bottom) and pretreated with or without ML-7 (25 μ M, 30 min) were exposed to an fMLP (10 μ M)-containing micropipette and allowed to migrate for the times indicated. Fluorescence of each probe and the corresponding DIC images are shown. Bar, 10 μ m. **(B)** Spatial distribution and line profiles of actin-YFP, PAK-PBD-YFP, and PH-AKT-GFP gradients in dHL-60 cells exposed to fMLP (10 μ M), delivered from a micropipette (white dot indicates the beginning of the measurement) for ~ 240 s. Cells were not pretreated (top) or were pretreated with ML-7 (bottom). A graph below each image plots fluorescence intensity of each probe (y axis) versus distance (x axis) for the corresponding cell. **(C)** Relative accumulation of actin-YFP, PAK-PBD-YFP, and PH-AKT-GFP at the leading edge of dHL-60 cells exposed to fMLP (10 μ M), delivered from a micropipette. Leading edge (L) in fluorescence image was demarcated by the corresponding DIC image and the rest of the cell was defined as cell body (C). Cells were pretreated with or without ML-7. For control cells, 3 min after the attractant exposure was chosen for analysis. For treated cells, a time point when the

pseudopod extension is at its peak was selected. Each bar in the graph below represents the ratio of mean fluorescence intensity between the leading edge and cell body. Values are normalized to the ratio of mean fluorescence intensity in control cells (=100%) and are means \pm SEM (n is shown within each bar). Results significantly different from those of control are indicated by asterisks (*, $p < 0.001$; **, $p < 0.0001$).

Supplementary Figure S9. PSD plots of tractions at the leading (left panel) and the trailing edge (right panel) of three dHL-60 cells pretreated with ML-7 (30 μ M, 30 min) (**A**), with MLCK depleted (**B**) or pretreated with Y-27632 (100 μ M, 30 min) (**C**). Traction values from three cells were analyzed and combined in one plot. See Figure 4 legends for more details.

Supplementary Figure S10. PSD plots of tractions at the leading (left panel) and the trailing edge (right panel) of primary neutrophils pretreated with ML-7 (30 μ M, 30 min) (**A**), or Y-27632 (100 μ M, 30 min) (**B**). 6 cells were analyzed for each treatment, and a representative cell is shown. Cells were on a substrate of 3.5 kPa stiffness.

Supplementary Figure S11. PSD plots of tractions at the leading (left panel) and the trailing edge (right panel) of a migratory primary neutrophil pretreated with blebbistatin (100 μ M, 30 min) (**A**) or ML-7 (25 μ M, 30 min) (**B**). Cells were allowed to migrate toward chemoattractant-containing micropipette (fMLP, 10 μ M) on a fibronectin-coated polyacrylamide gel (100 kPa) for 4-5 min. 6 cells were analyzed for each condition, and a representative cell is shown.

Supplementary Figure S12. (A) A dHL-60 cell bathed in RAD (top) or RGD peptides (50 $\mu\text{g/ml}$) (bottom) was exposed to a point source of fMLP (10 μM in the micropipette) for the times indicated. (B) Higher magnification DIC images of two migrating cells show characteristic shapes of the leading edge either with RAD treatment (left) or with RGD treatment (right). (C) dHL-60 cells bathed in either RAD or RGD peptides (50 $\mu\text{g/ml}$) were exposed to a chemotactic gradient delivered from a micropipette containing 10 μM fMLP for 10 min. The cells were assessed for their ability to establish or maintain polarity toward the micropipette throughout the observed time period. The result is shown in the graph ($n = 43$ for RAD-treated cells, 48 for RGD-treated cells). All bars = 10 μm .

Supplementary Figure S13. dHL-60 cells were transfected with EGFP- $\alpha 5$ -integrin and exposed to a point source of 10 μM fMLP (from micropipette) for the indicated times. TIRF (488 nm) and the corresponding DIC images are shown. Cells were not pretreated (A) pretreated with ML-7 (B), Blebbistatin (C) and Y-27632 (D). Leading-edge attachment of control cells was indicated by the GFP fluorescence; nearly no signals were detected at the leading edges in cells treated with ML-7 or blebbistatin. Leading edges in the TIRF images are marked by yellow lines. Yellow arrows indicate the direction of chemoattractant gradient. Black arrows point to the long stretched trailing edges. All bars = 10 μm .

Supplementary Figure S14. (A) A single, non-stimulated dHL-60 cell, pretreated with or without ML-7 (25 μM , 30 min), was held with a pipette and exposed to a gradient from 10 μM fMLP from a delivery pipette. Before exposure to fMLP, the cell was spherical (i). Within 20 s, a pseudopod started to grow (ii). The pseudopod extended until a maximal length was reached (iii and iv), and then it started to retract (v and vi). Bar, 10 μm . (B) The growth of pseudopod as a function of time.

Pseudopod formation was stimulated with delivery of 10 μ M fMLP from a pipette as shown in **(A)**. Chemoattractant delivery started at time 0. Values are means \pm SEM (n=6). **(C)** Quantification of F-actin polymerization. Cells pretreated with or without ML-7 were stimulated with fMLP (1 μ M) for various times in suspension and fixed for staining with rhodamine-phalloidin. Fluorescence in stained cells was determined by flow cytometry. Values are means \pm SEM (n = 4). **(D)** Quantification of Rac-GTP in dHL-60 cells with or with ML-7 treatment. Cells were pretreated with ML-7, stimulated with fMLP (1 μ M) for times indicated and lysed. The level of Rac-GTP was determined by the use of an absorbance-based Rac G-LISA kit. The y axis represents relative absorbance normalized to the signal (=1) detected in the control cells without ML-7 treatment. Each bar represents the mean \pm SEM (error bars) (n =4). **(E)** dHL-60 cells pretreated with or without ML-7 were stimulated for indicated times in suspension and lysed. Akt phosphorylation (Ser473) was assessed by western blotting. Values are normalized to the level in control cells without fMLP stimulation (=1) and are means \pm SEM (n=8). Representative blots for phospho- and total Akt are shown (left panel). **(F)** dHL-60 cells were fixed, incubated with GST, fixed and stained with an anti-GST antibody and anti- α 5-integrin antibody. The procedure was performed as described in Figure 6C legends, except that GST was used. The yellow arrow points to the leading edge. Bar, 10 μ m.

TEXT FOR SUPPLEMENTARY MOVIES

Supplementary Movie S1 (traction map) shows the responses of a control dHL-60 cell to a point source of fMLP. Some of the time points are shown in Figure 1A in the text. The total time is 290 sec.

Supplementary Movie S2 (fluorescence channel) and Supplementary Movie S3 (DIC channel) show the responses of a dHL-60 cell expressing mCherry-tagged myosin IIA to a point source of fMLP. Some of the time points are shown in Figure 2B in the text.

Supplementary Movie S4 (green fluorescence channel) and Supplementary Movies S5 (red fluorescence channel) show 3 dimensional views of a polarized dHL-60 cell stained with Alexa fluor 488 phalloidin to localize F-actin (green; Movie S4) and a specific antibody against myosin IIA (red; Movie S5). The schematic views are shown in Figure S2B.

Supplementary Movie S6 (DIC channel) shows the responses of control dHL-60 cells to a point source of fMLP. Some of the time points are shown in Figure 2F in the text.

Supplementary Movie S7 (DIC channel) shows the responses of blebbistatin-treated dHL-60 cells to a point source of fMLP. Some of the time points are shown in Figure 2F in the text.

Supplementary Movie S8 (DIC channel) shows the responses of myosin IIA-depleted dHL-60 cells to a point source of fMLP. Some of the time points are shown in Figure 2F in the text.

Supplementary Movie S9 (DIC channel) shows the responses of Y-27632-treated dHL-60 cells to a point source of fMLP. Some of the time points are shown in Figure 2F in the text.

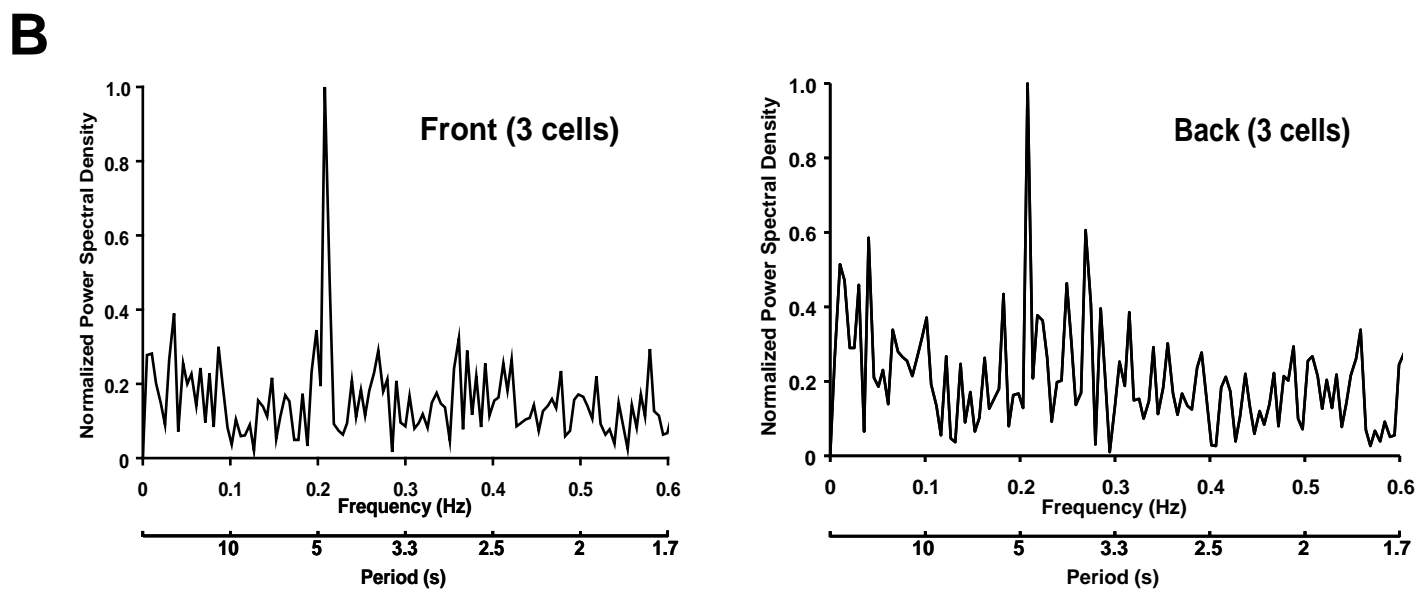
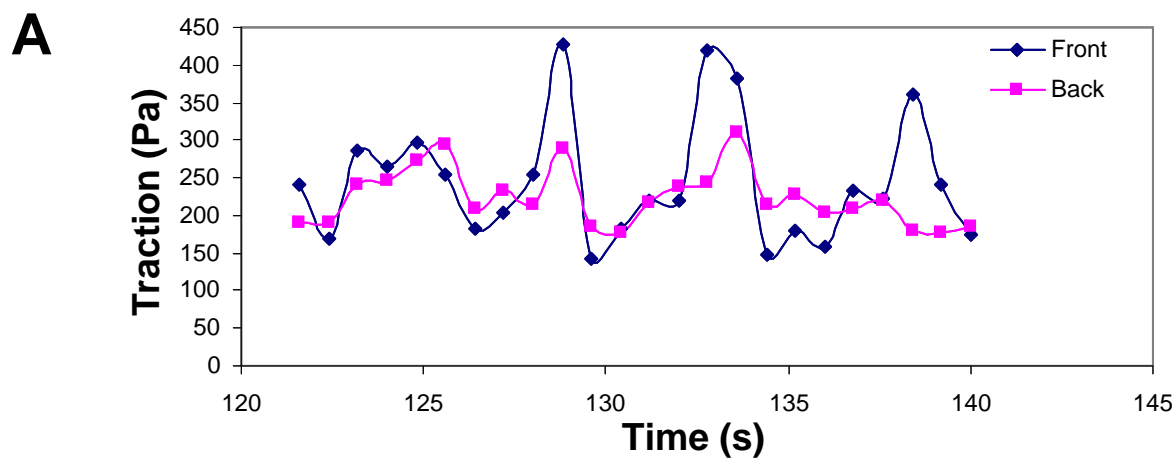
Supplementary Movie S10 (GFP channel) and Supplementary Movie S11 (DIC channel) show the responses of dHL-60 cells expressing sMLCK-GFP to a uniform concentration of fMLP. Some of the time points are shown in Figure S4B in the Supplementary Information.

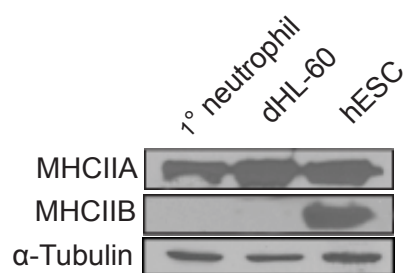
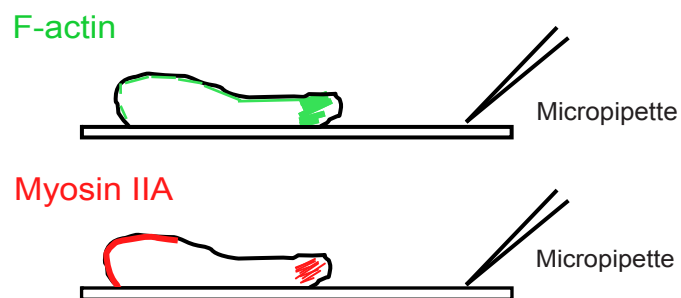
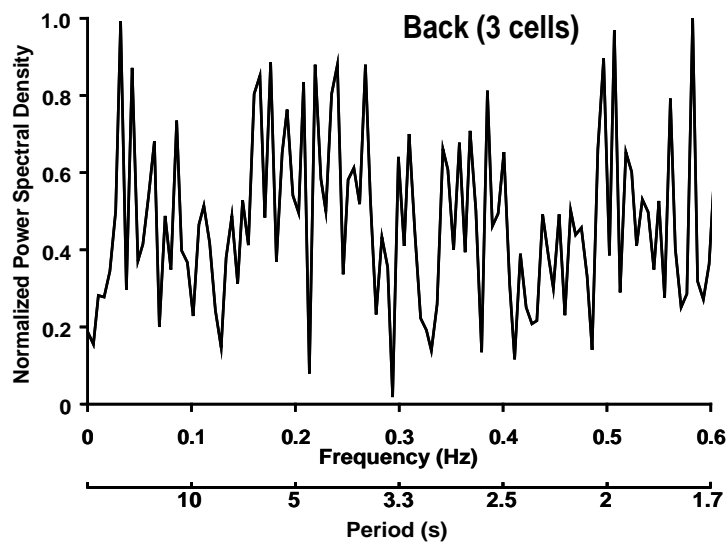
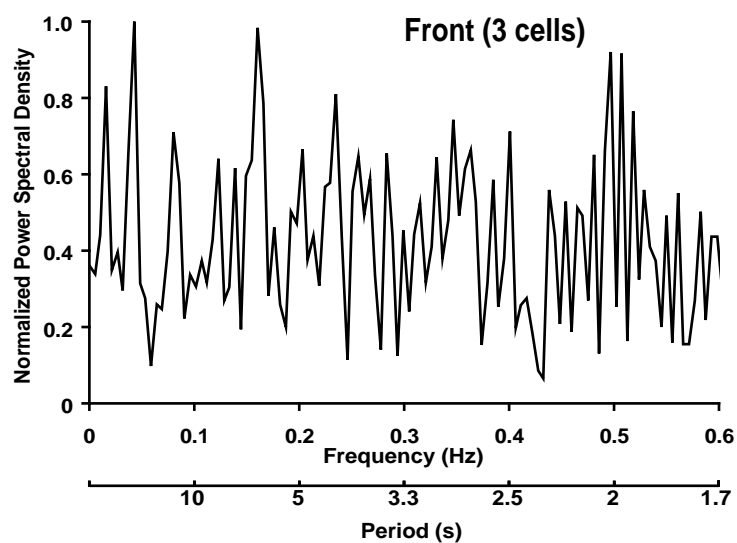
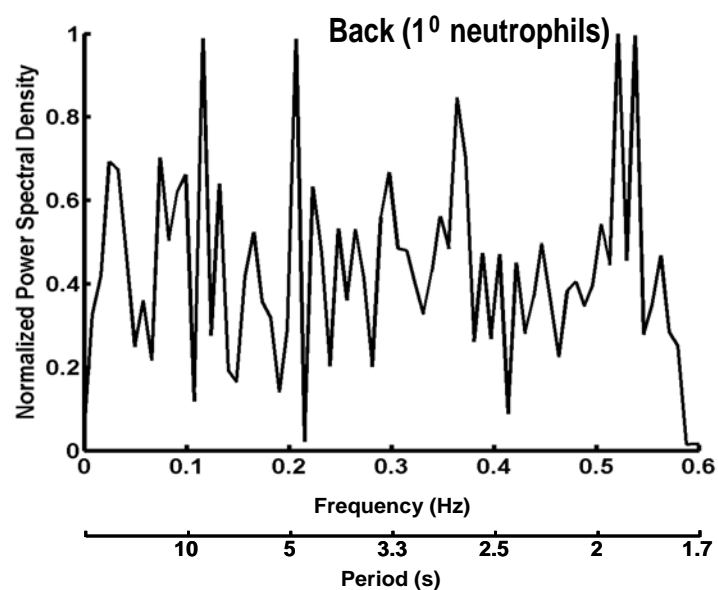
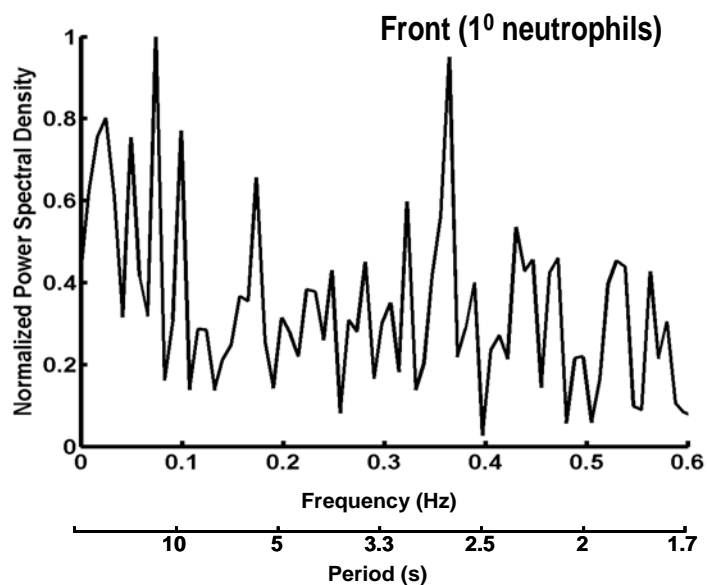
Supplementary Movie S12 (traction map) shows the responses of a MLCK-depleted dHL-60 cell to a point source of fMLP. Some of the time points are shown in Figure 4A in the text. The total time is 290 sec.

SUPPLEMENTARY REFERENCES

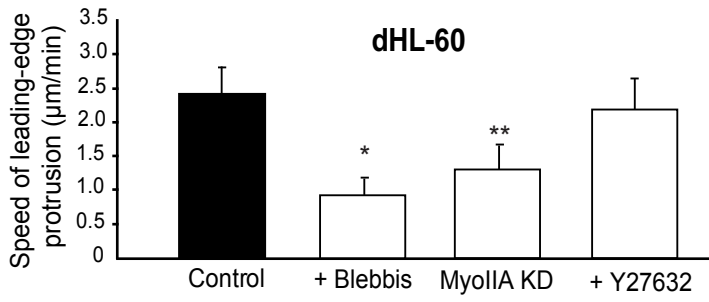
1. Wilson AK, Gorgas G, Claypool WD, de Lanerolle P. An increase or a decrease in myosin II phosphorylation inhibits macrophage motility. *J Cell Biol.* 1991;114:277-283.
2. Poperechnaya A, Varlamova O, Lin PJ, Stull JT, Bresnick AR. Localization and activity of myosin light chain kinase isoforms during the cell cycle. *J Cell Biol.* 2000;151:697-708.
3. Laukaitis CM, Webb DJ, Donais K, Horwitz AF. Differential dynamics of alpha 5 integrin, paxillin, and alpha-actinin during formation and disassembly of adhesions in migrating cells. *J Cell Biol.* 2001;153:1427-1440.
4. Vicente-Manzanares M, Zareno J, Whitmore L, Choi CK, Horwitz AF. Regulation of protrusion, adhesion dynamics, and polarity by myosins IIA and IIB in migrating cells. *J Cell Biol.* 2007;176:573-580.
5. Xu J, Wang F, Van Keymeulen A, et al. Divergent signals and cytoskeletal assemblies regulate self-organizing polarity in neutrophils. *Cell.* 2003;114:201-214.
6. Wang F, Herzmark P, Weiner OD, Srinivasan S, Servant G, Bourne HR. Lipid products of PI(3)Ks maintain persistent cell polarity and directed motility in neutrophils. *Nat Cell Biol.* 2002;4:513-518.
7. Orr AW, Ginsberg MH, Shattil SJ, Deckmyn H, Schwartz MA. Matrix-specific Suppression of Integrin Activation in Shear Stress Signaling. *Mol Biol Cell.* 2006;17:4686-4697.
8. Fumagalli L, Zhang H, Baruzzi A, Lowell CA, Berton G. The Src Family Kinases Hck and Fgr Regulate Neutrophil Responses to N-Formyl-Methionyl-Leucyl-Phenylalanine. *J Immunol.* 2007;178:3874-3885.
9. Weiner OD, Rentel MC, Ott A, et al. Hem-1 complexes are essential for Rac activation, actin polymerization, and myosin regulation during neutrophil chemotaxis. *PLoS Biol.* 2006;4:e38.
10. Ryu H, Lee JH, Kim KS, Jeong SM, Kim PH, Chung HT. Regulation of neutrophil adhesion by pituitary growth hormone accompanies tyrosine phosphorylation of Jak2, p125FAK, and paxillin. *J Immunol.* 2000;165:2116-2123.
11. Zhelev DV, Alteraifi AM, Chodniewicz D. Controlled pseudopod extension of human neutrophils stimulated with different chemoattractants. *Biophys J.* 2004;87:688-695.
12. Smith A, Bracke M, Leitinger B, Porter JC, Hogg N. LFA-1-induced T cell migration on ICAM-1 involves regulation of MLCK-mediated attachment and ROCK-dependent detachment. *J Cell Sci.* 2003;116:3123-3133.
13. Gupta N, DeFranco AL. Visualizing lipid raft dynamics and early signaling events during antigen receptor-mediated B-lymphocyte activation. *Mol Biol Cell.* 2003;14:432-444.
14. Xu J, Gao XP, Ramchandran R, Zhao YY, Vogel SM, Malik AB. Nonmuscle myosin light-chain kinase mediates neutrophil transmigration in sepsis-induced lung inflammation by activating beta2 integrins. *Nat Immunol.* 2008;9:880-886.
15. Srinivasan S, Wang F, Glavas S, et al. Rac and Cdc42 play distinct roles in regulating PI(3,4,5)P3 and polarity during neutrophil chemotaxis. *J Cell Biol.* 2003;160:375-385.
16. Servant G, Weiner OD, Herzmark P, Balla T, Sedat JW, Bourne HR. Polarization of chemoattractant receptor signaling during neutrophil chemotaxis. *Science.* 2000;287:1037-1040.

17. Totsukawa G, Wu Y, Sasaki Y, et al. Distinct roles of MLCK and ROCK in the regulation of membrane protrusions and focal adhesion dynamics during cell migration of fibroblasts. *J Cell Biol.* 2004;164:427-439.
18. Webb DJ, Donais K, Whitmore LA, et al. FAK-Src signalling through paxillin, ERK and MLCK regulates adhesion disassembly. *Nat Cell Biol.* 2004;6:154-161.
19. Ridley AJ, Schwartz MA, Burridge K, et al. Cell migration: integrating signals from front to back. *Science.* 2003;302:1704-1709.
20. Staffan Johansson GS, Krister Wennerberg, Annika Armulik, Lars Lohikangas. Fibronectin-Integrin Interactions. *Frontiers in Bioscience* 1997;2:126-146.

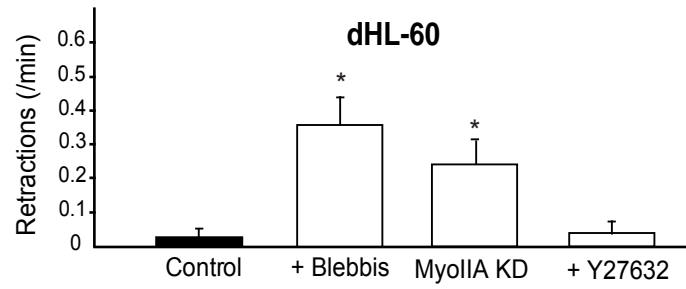


A**B****C****D**

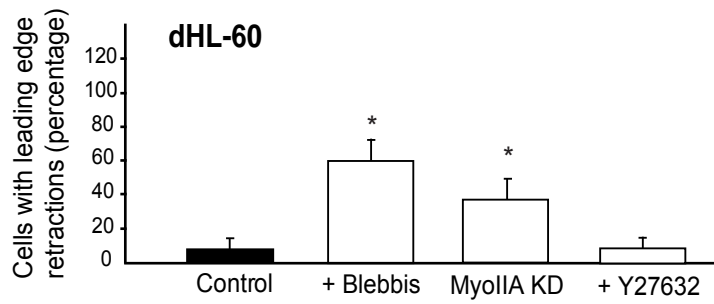
A



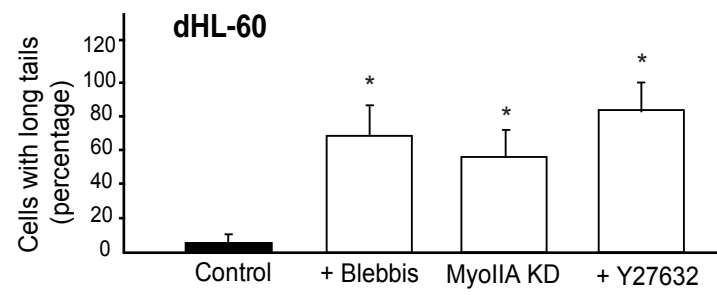
B



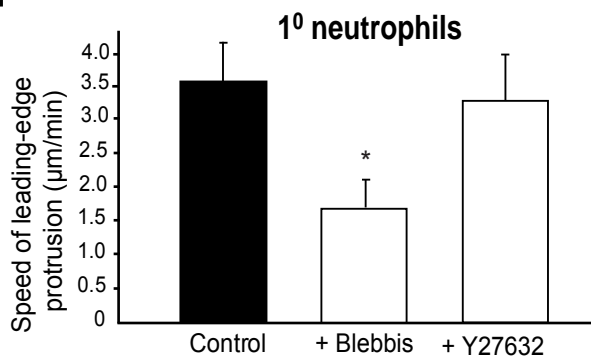
C



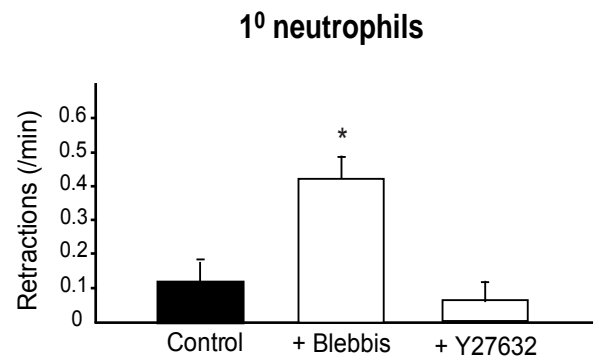
D



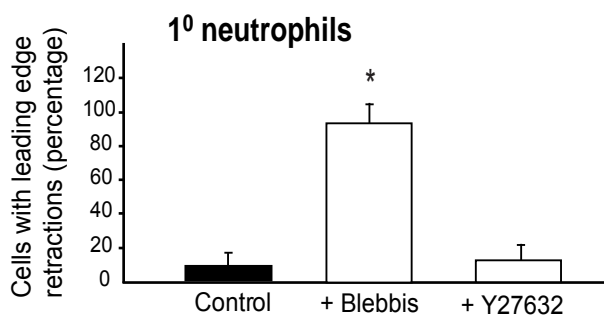
E



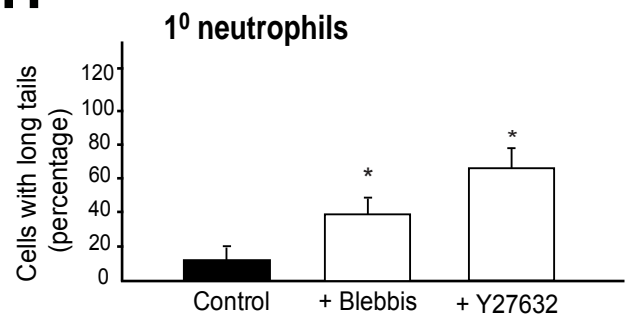
F



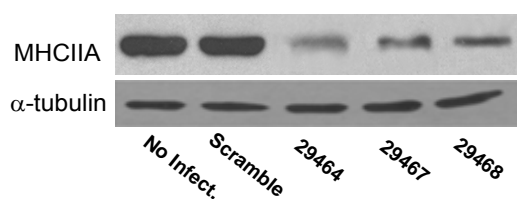
G

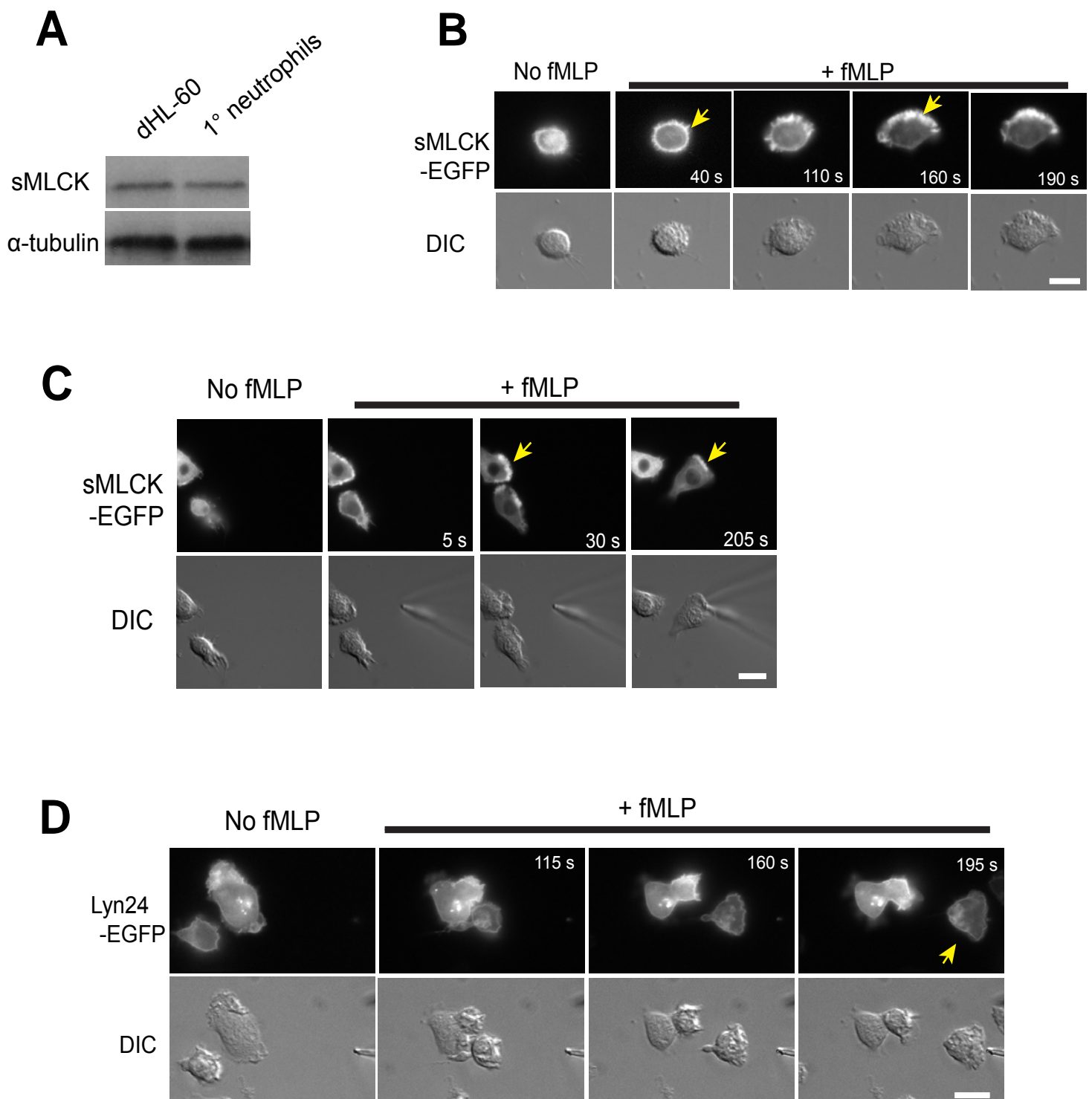


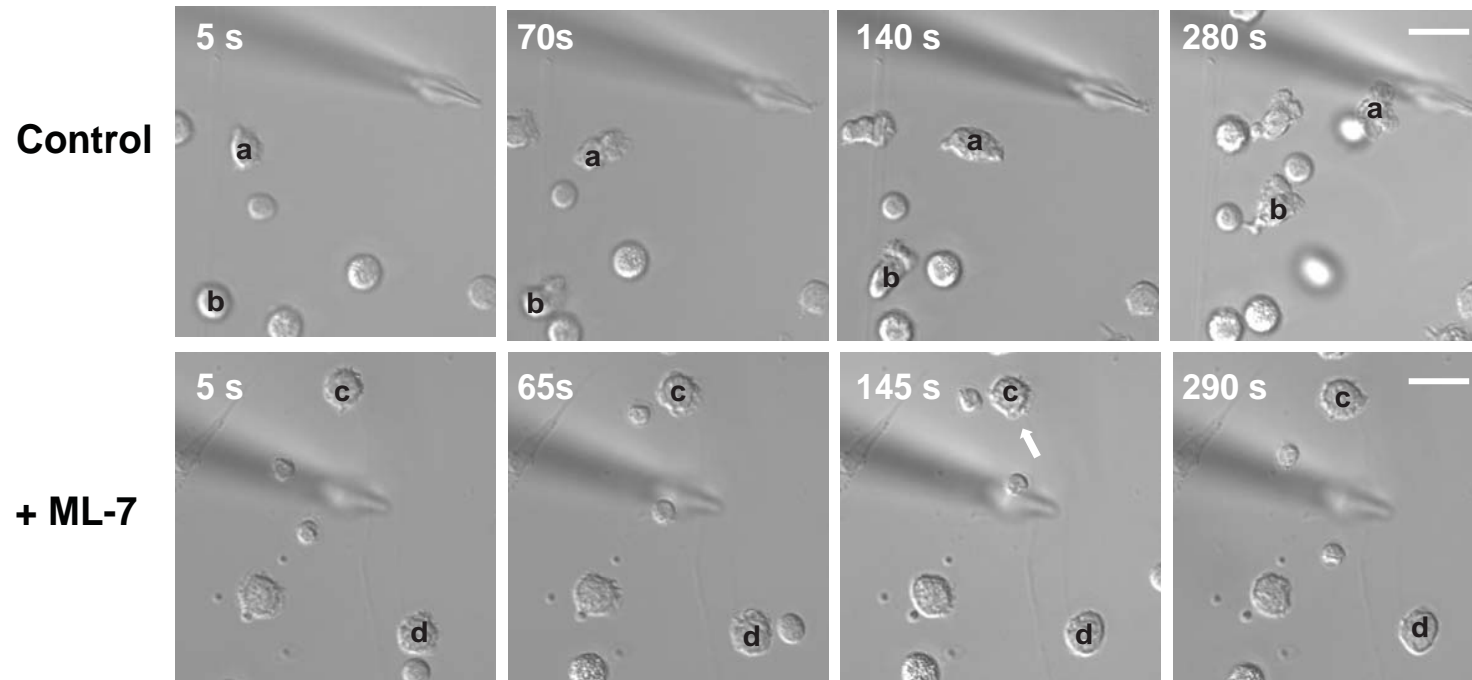
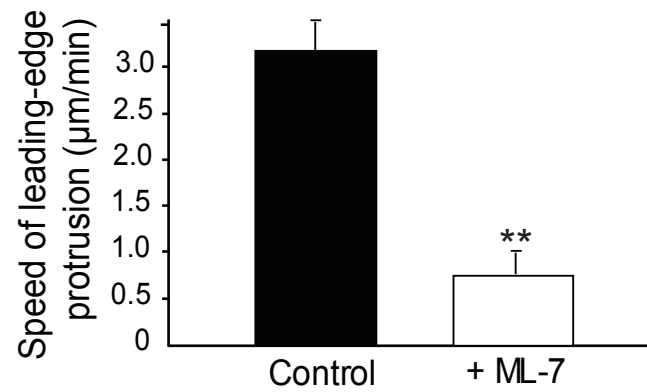
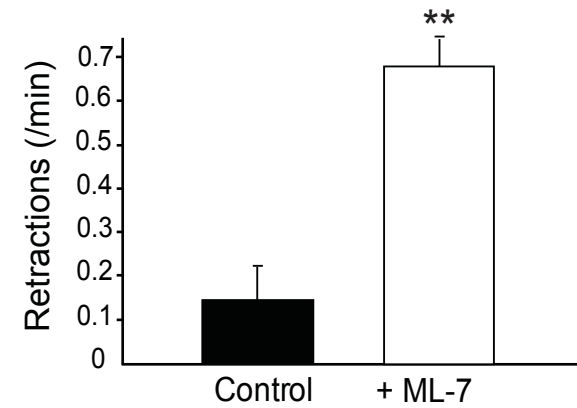
H

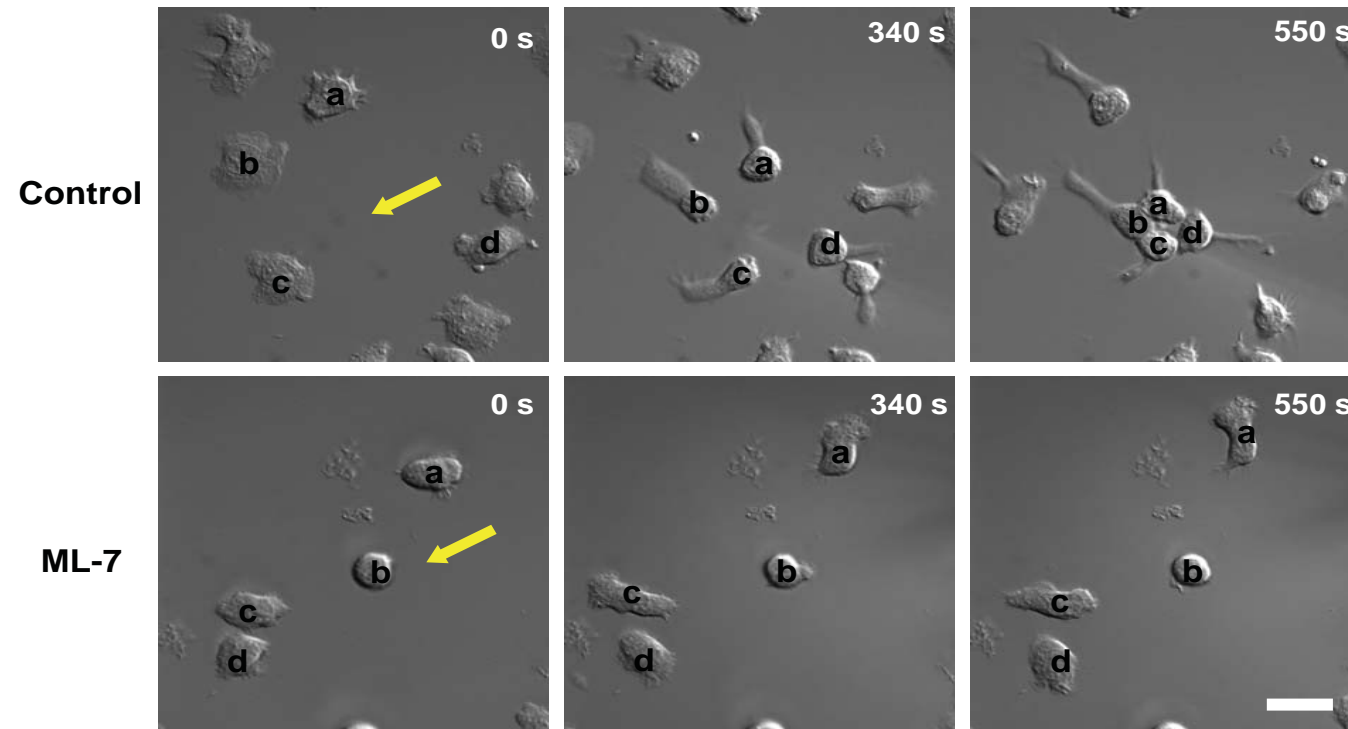
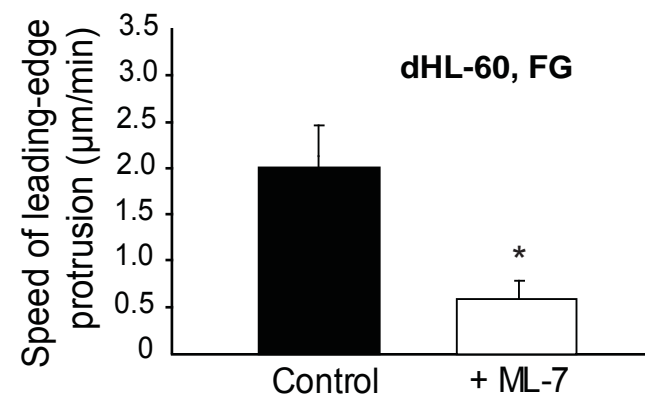
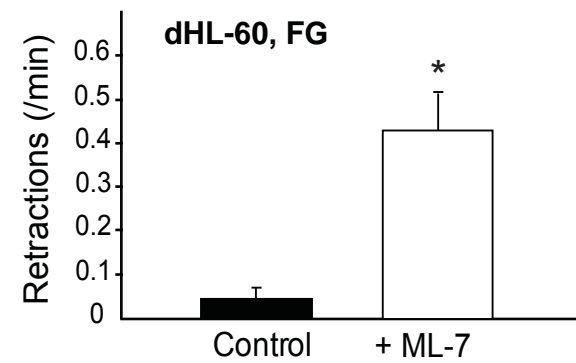


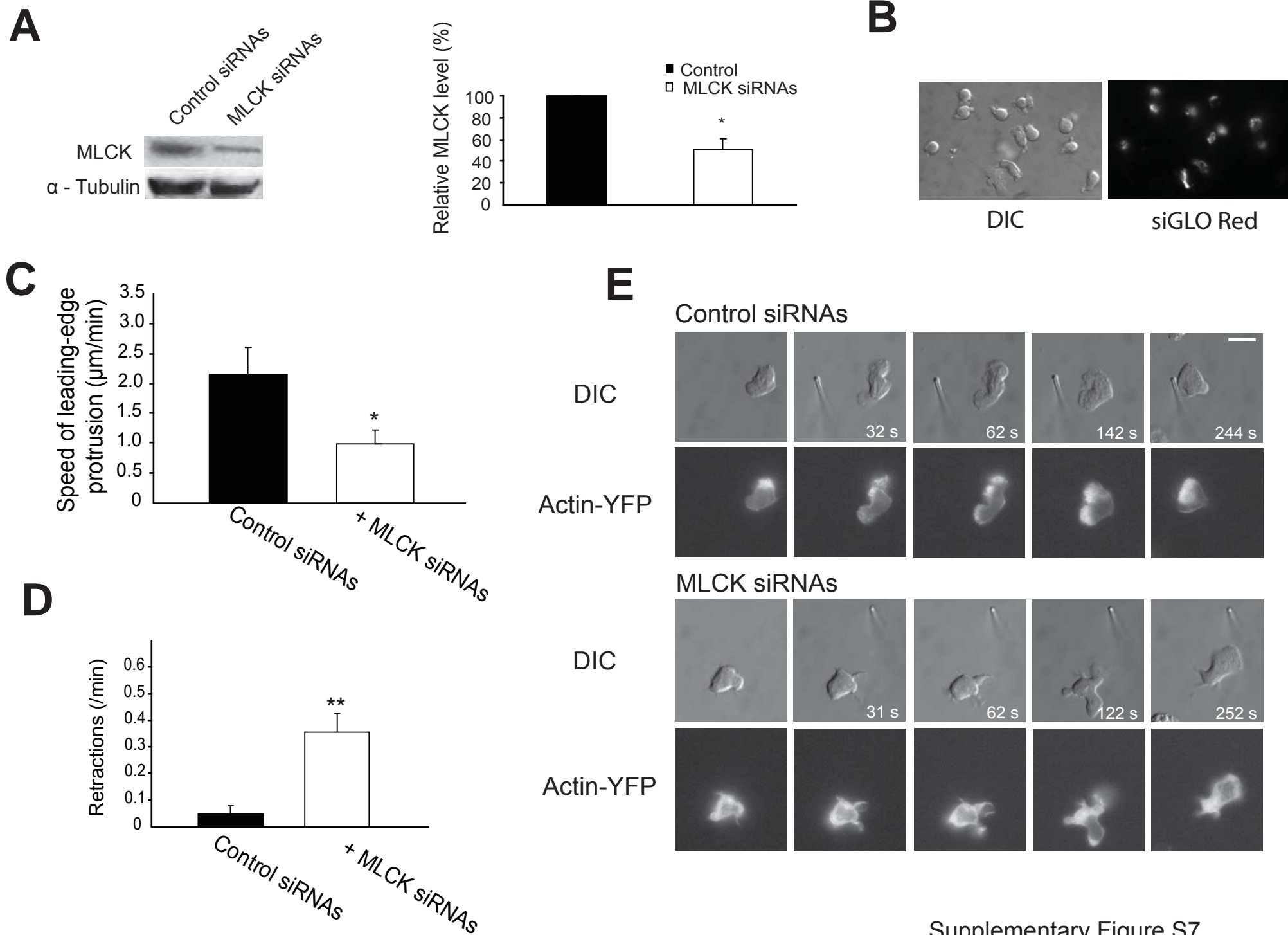
I





A**Primary neutrophils****B****C**

A**dHL-60, FG****B****C**



Supplementary Figure S7

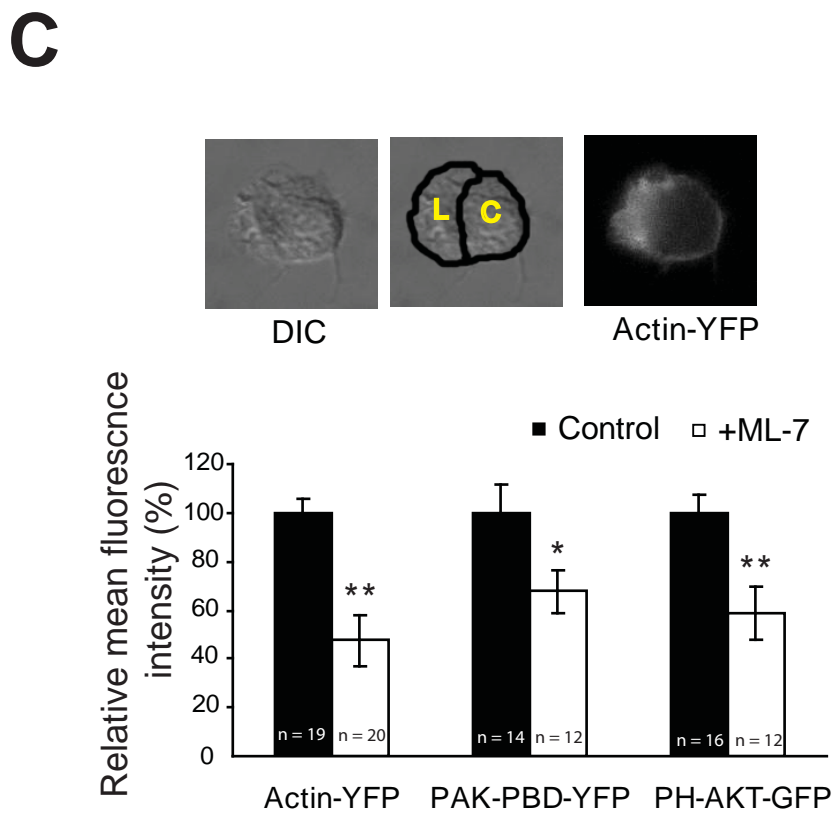
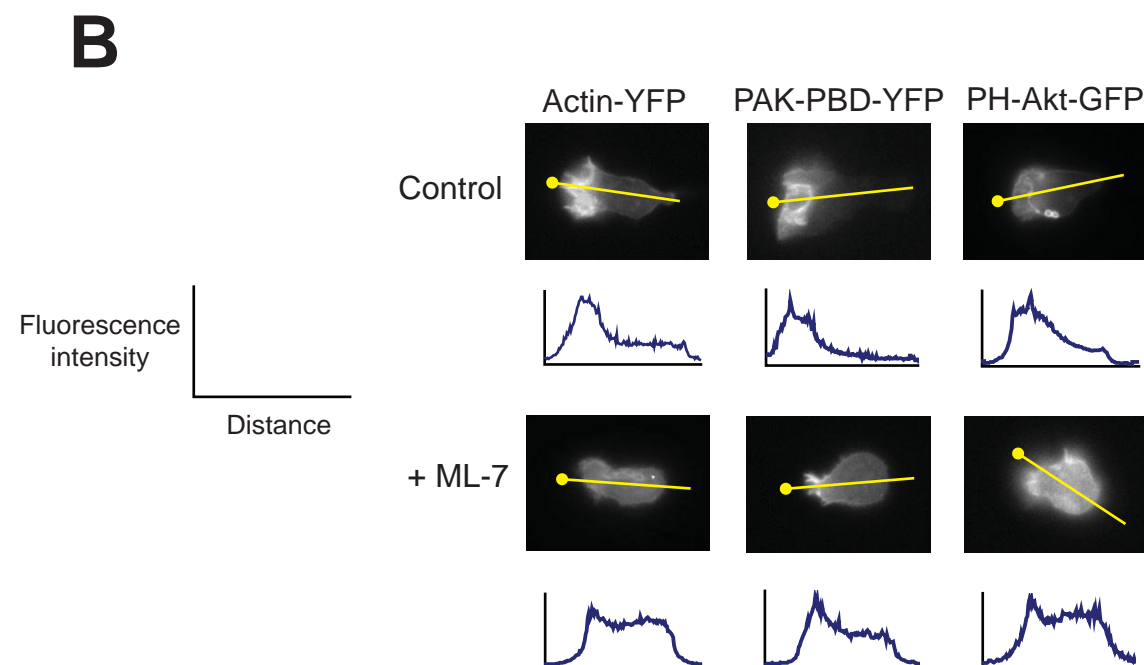
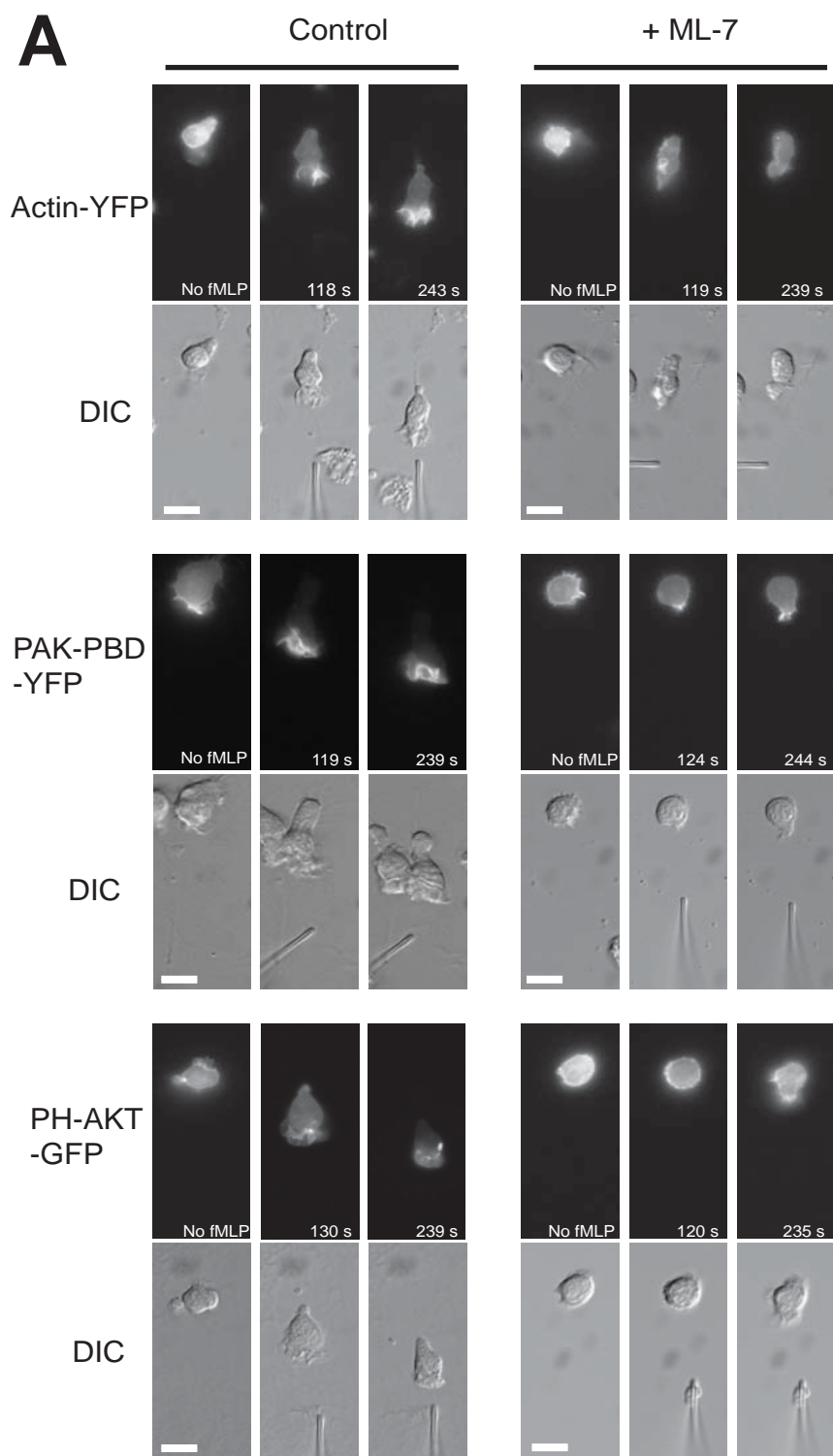
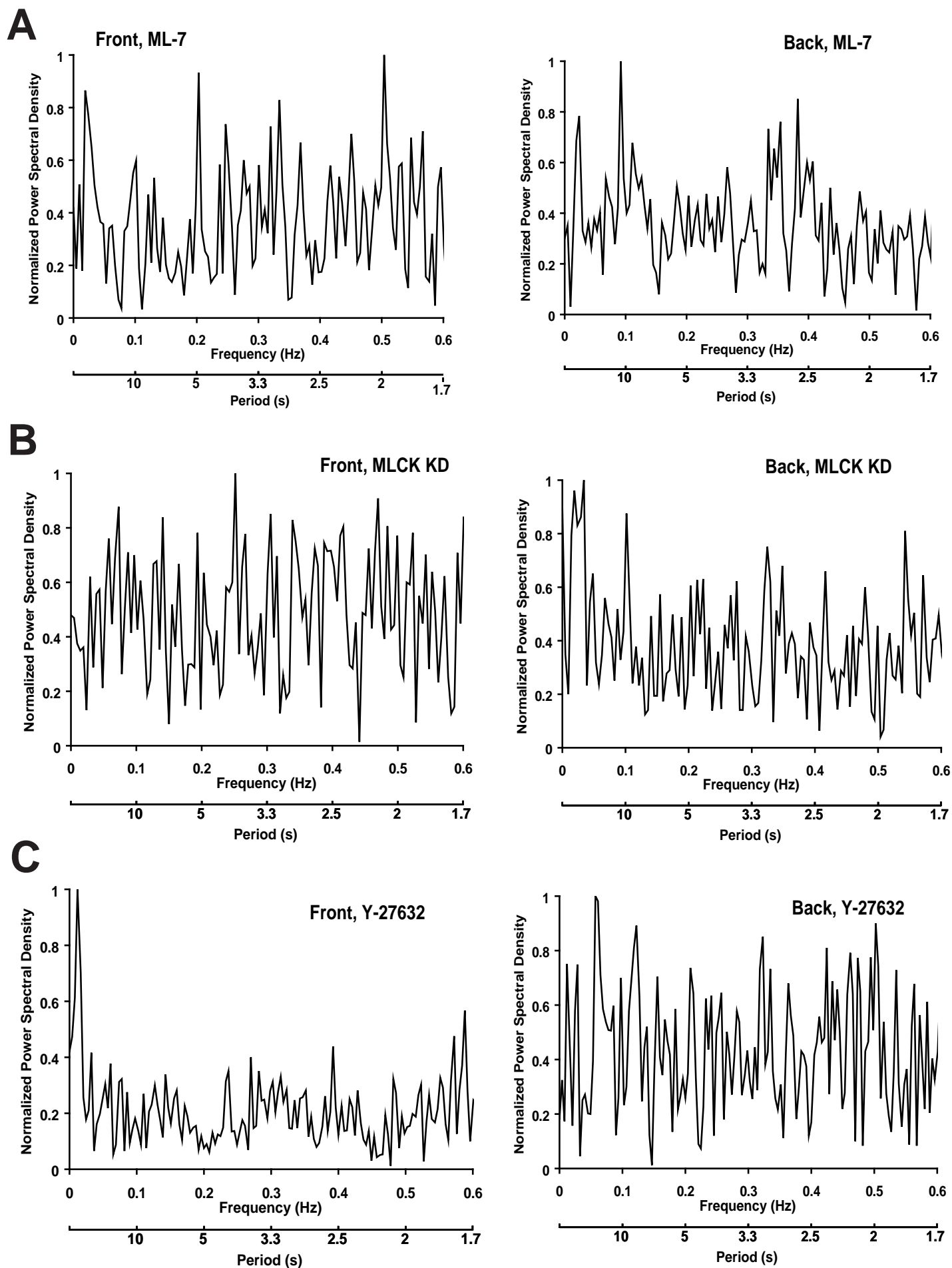


Figure S8

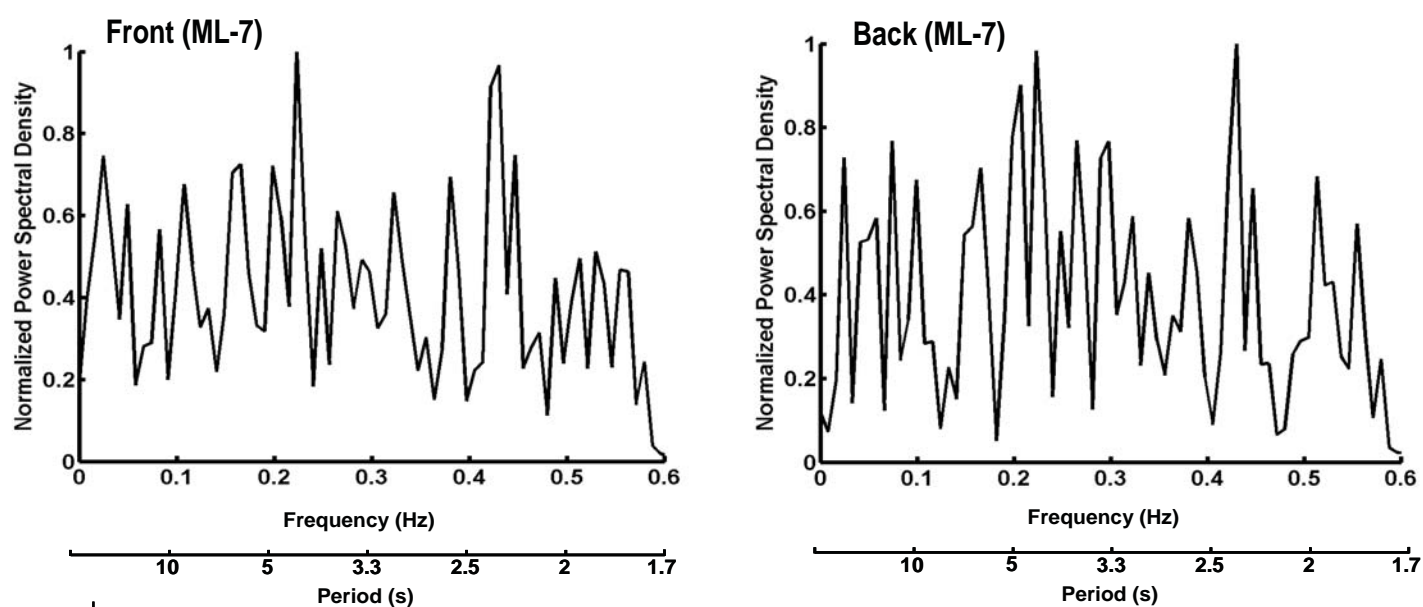
Figure S9

dHL-60 cells



Primary neutrophils, 3.5 kPa

A



B

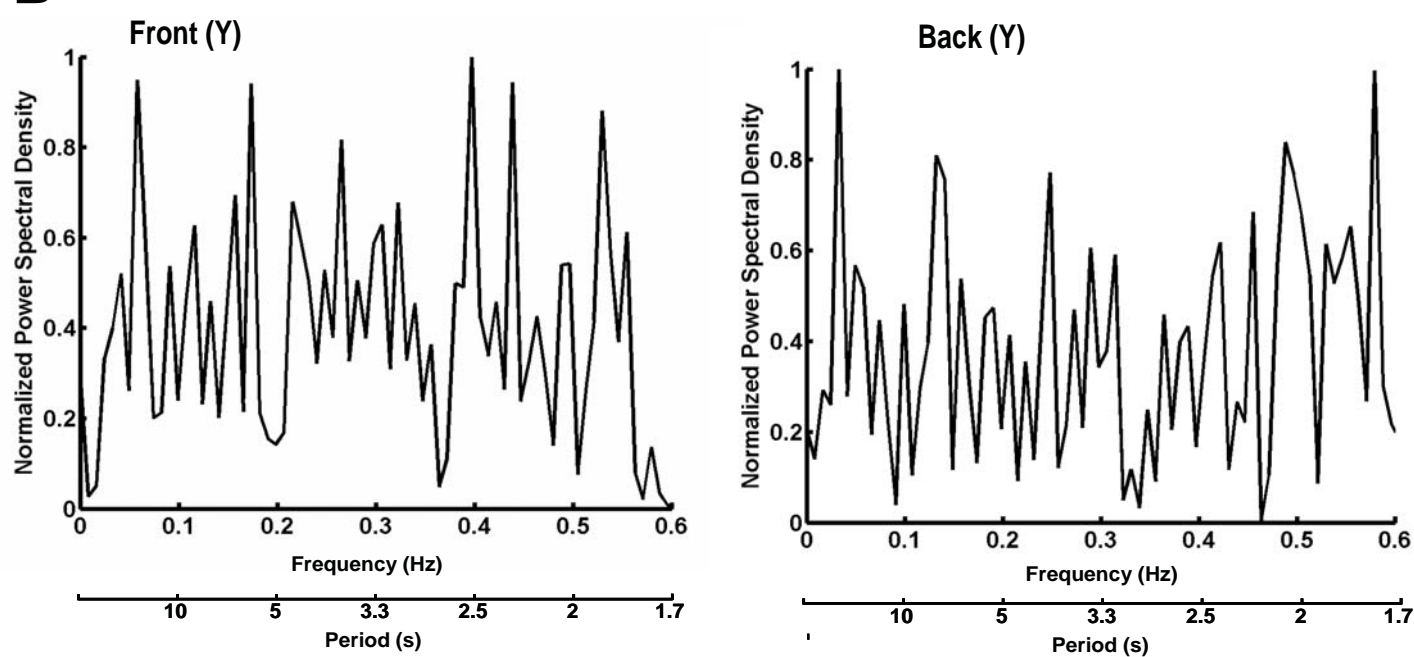
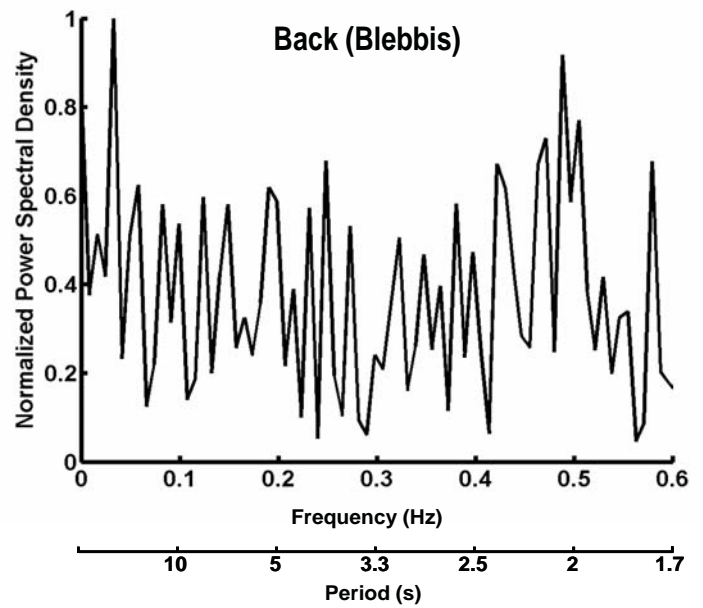
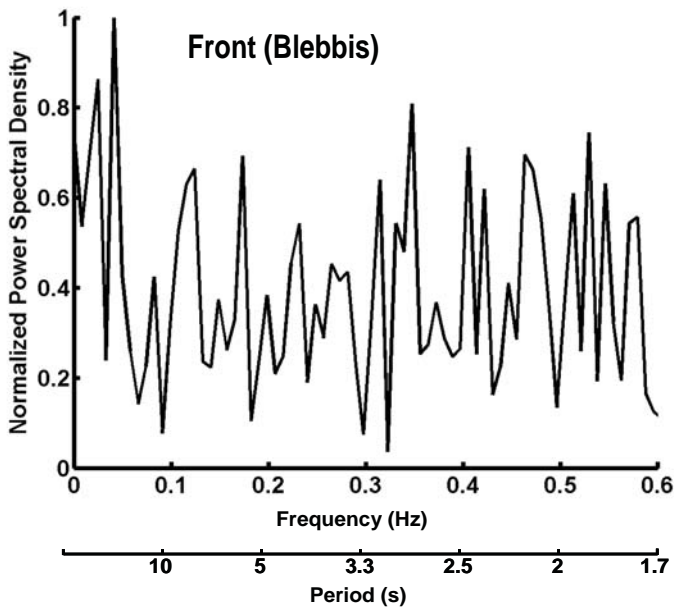


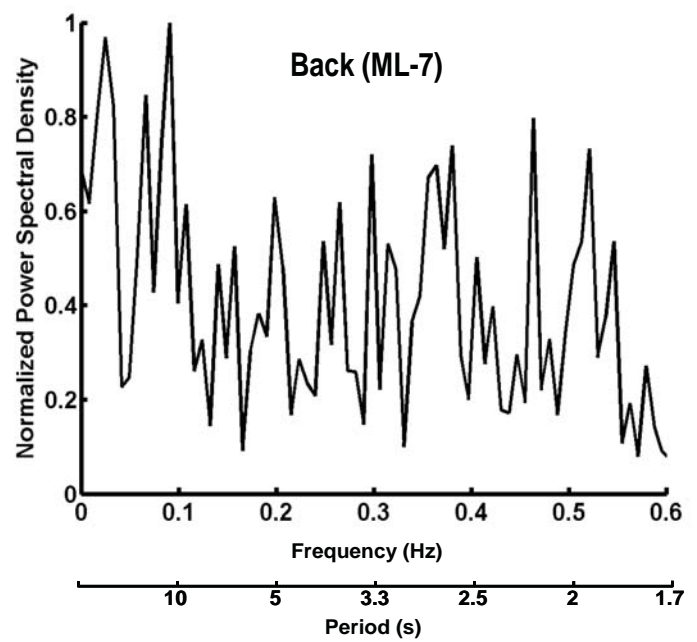
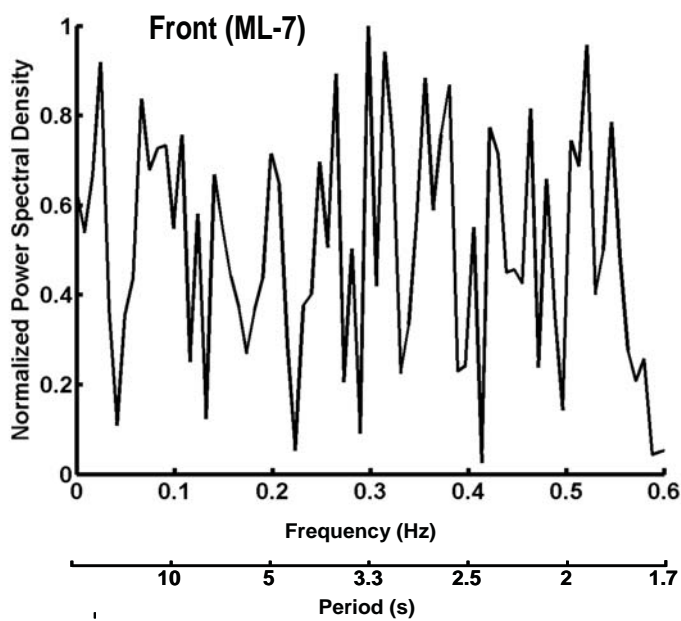
Fig. S10

Primary neutrophils, 100 kPa

A

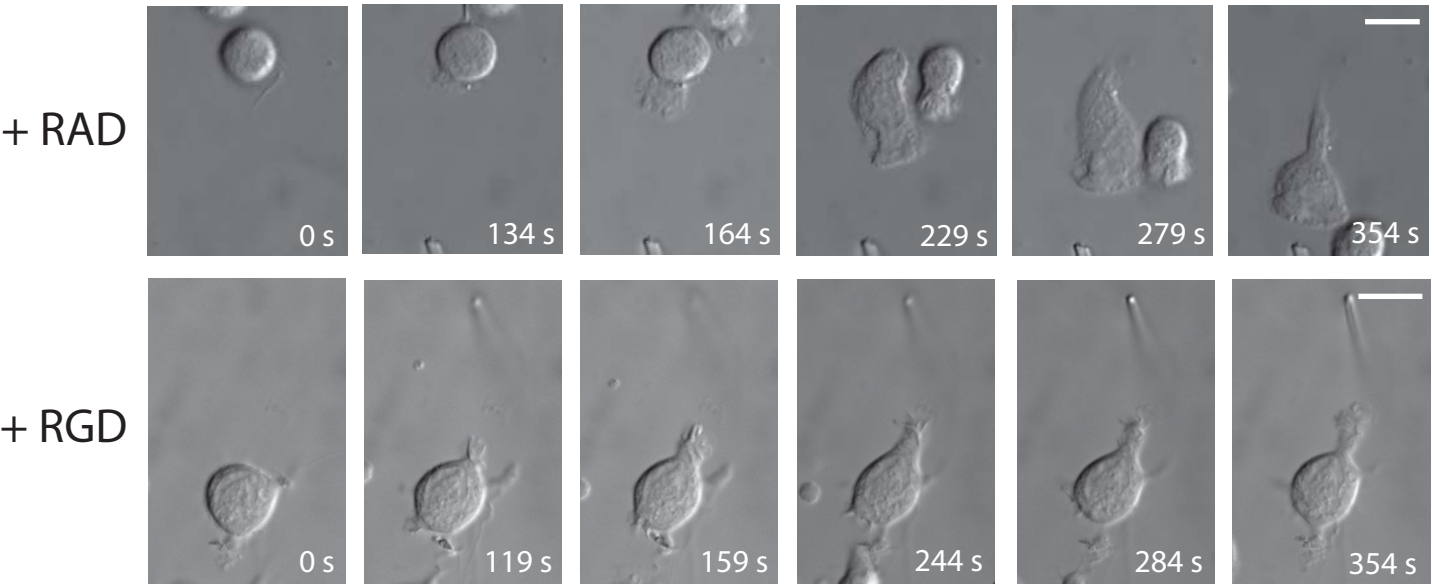


B

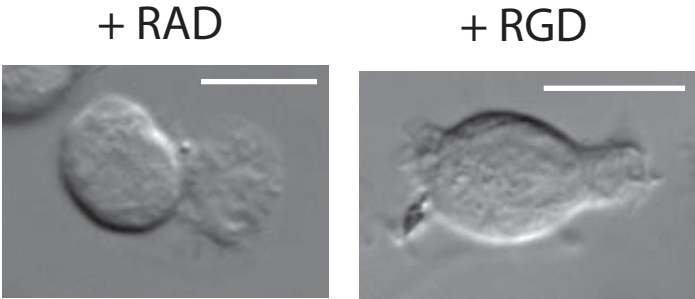


Supplementary Figure S12

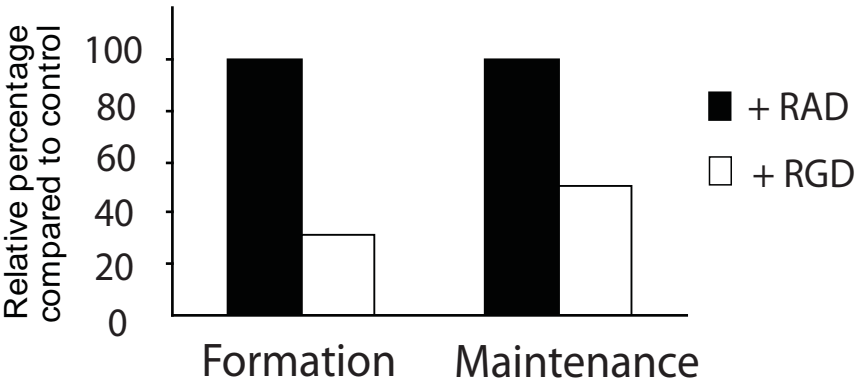
A



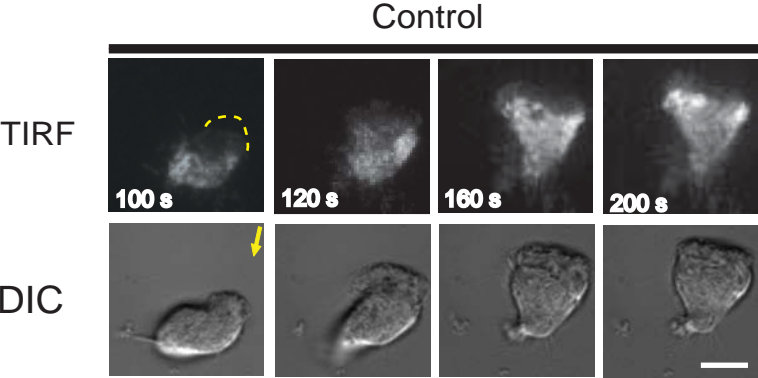
B



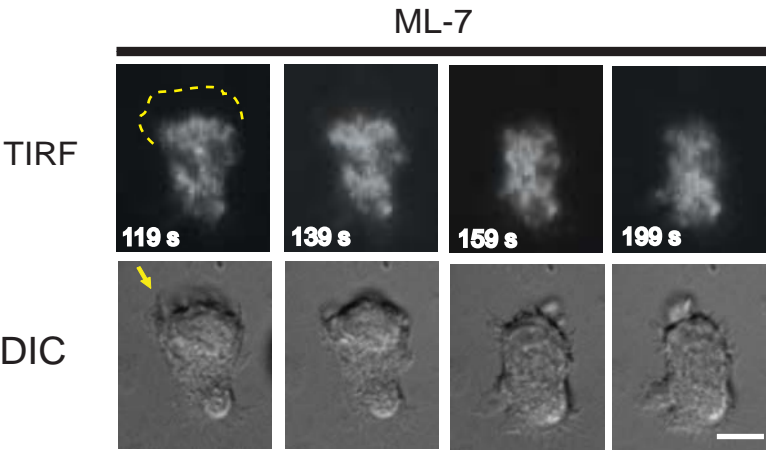
C



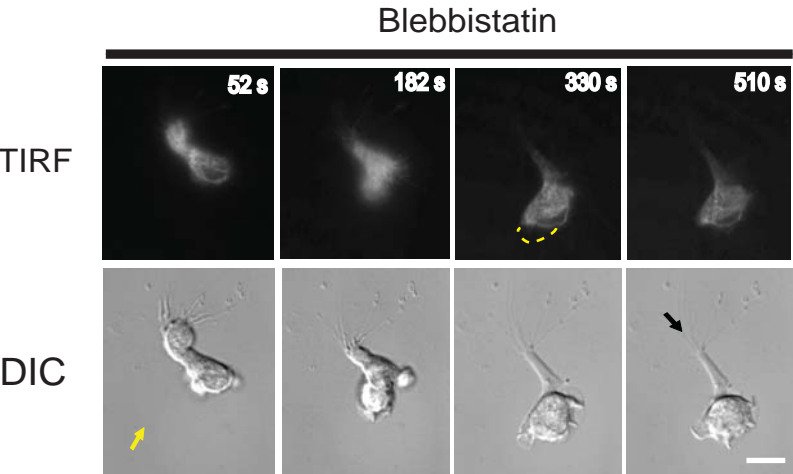
A



B



C



D

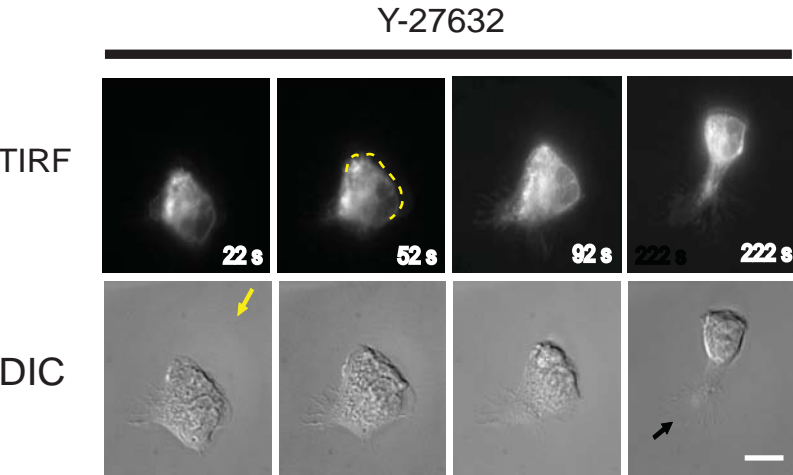


Figure S14

